Dimension dependence of clustering dynamics in models of ballistic aggregation and freely cooling granular gas

Subhajit Paul and Subir K. Das*

Theoretical Sciences Unit, Jawaharlal Nehru Centre for Advanced Scientific Research, Jakkur P.O., Bangalore 560064, India

(Received 6 September 2017; revised manuscript received 8 January 2018; published 26 March 2018)

Via event-driven molecular dynamics simulations we study kinetics of clustering in assemblies of inelastic particles in various space dimensions. We consider two models, viz., the ballistic aggregation model (BAM) and the freely cooling granular gas model (GGM), for each of which we quantify the time dependence of kinetic energy and average mass of clusters (that form due to inelastic collisions). These quantities, for both the models, exhibit power-law behavior, at least in the long time limit. For the BAM, corresponding exponents exhibit strong dimension dependence and follow a hyperscaling relation. In addition, in the high packing fraction limit the behavior of these quantities become consistent with a scaling theory that predicts an inverse relation between energy and mass. On the other hand, in the case of the GGM we do not find any evidence for such a picture. In this case, even though the energy decay, irrespective of packing fraction, matches quantitatively with that for the high packing fraction picture of the BAM, it is inversely proportional to the growth of mass only in one dimension, and the growth appears to be rather insensitive to the choice of the dimension, unlike the BAM.

DOI: 10.1103/PhysRevE.97.032902

I. INTRODUCTION

Growth in many physical situations occurs due to inelastic collisions among particles or aggregates [1–20]. Typical examples [1,4,7,9–12,14,16–18,21–23] are growth of liquid droplets and solid clusters in upper atmosphere, clustering in cosmic dust, etc. In this context, two simple models, referred to as the ballistic aggregation model (BAM) [1,4,24] and the granular gas model (GGM) [13], have been of much theoretical interest. Both the models are classic examples of dissipative systems and exhibit clustering phenomena. The understanding of the decay of kinetic energy (E) and the growth of average mass (m) of clusters in these models is of significant importance.

In the BAM, spherical hard particles move with constant velocities and merge upon collisions to form larger aggregates, by keeping the shape unchanged. In this process, mass and momentum of the system remain conserved, whereas the (kinetic) energy decays. It is, of course, understood that following collisions fractal structures will emerge [7,25] in space dimension $d > 1$. Even though it appears a bit unrealistic from that point of view, this simple model can provide important insights into the understanding of growth in many complex systems [1,4–6,24]. In fact, in many situations colliding objects undergo deformation and so, if the collision interval is long, the above mentioned spherical structural approximation is reasonably good. In the case of the GGM, on the other hand, the colliding particles do not merge. There the coefficient of normal restitution (e) lies in the range $0 < e < 1$. Thus, following every collision, the particles lose a fraction $(1 - e^2)$ of the relative kinetic energy and move more parallel to each other. This leads to clustering phenomena [13,15,20,25–34], caused by shearing instability, with a stringlike pattern.

For the BAM, Carnevale, Pomeau, and Young (CPY) [1], via scaling arguments, predicted that

$$m \sim \frac{1}{E} \sim t^{2d/(d+2)}, \tag{1}$$

where t is the time. An inherent assumption in arriving at this quantitative picture is that the particle (or cluster) momenta are uncorrelated [26]. Even though the predictions in Eq. (1) are in agreement with the computer simulations in $d = 1$, discrepancies have been reported [4,25] for $d > 1$. Another theory in this context, by Trizac and Hansen [4], predicts the existence of a hyperscaling relation involving the time dependence of energy and mass. If one writes

$$E \sim t^{-\theta} \tag{2}$$

and

$$m \sim t^{\zeta}, \tag{3}$$

then the (positive) power-law exponents θ and ζ are expected to be connected to each other in d dimensions via [4]

$$2\zeta + d\theta = 2d. \tag{4}$$

While Eq. (1) satisfies the hyperscaling relation in Eq. (4), the former prediction is expected to be true, as stated above, when cluster momenta are uncorrelated, i.e., when collision frequency is high [24,25]. This latter picture will, thus, be valid when the particle density is reasonably large.

There have been efforts to check the validity of Eq. (4). Such works [4,25], however, restricted attention to $d = 2$. In this work we undertake a detailed study, by considering a wide range of density and adopting an accurate method of analysis, to confirm the hyperscaling relation of Eq. (4) in both $d = 2$ and 3. In this process we also intend to understand the convergence with respect to the validity of Eq. (1), in the above mentioned

*das@jncasr.ac.in

dimensions. Note that a detailed discussion of the theoretical prediction is given in the next section.

The literature related to GGM is more complex. Earlier theoretical and computational studies reported [33,34] the value of θ to be $d/2$. Soon after these works, simulations [28] in $d = 1$ showed that $\theta = 2/3$, which is in clear disagreement with this expectation. The latter number, in contrary, matches the CPY prediction. This led to the belief that there exists equivalence between the GGM and BAM. In fact further studies in $d = 1$, on growth and aging property [25], strengthen such a belief. However, the morphology for the GGM in higher dimensions is different from the BAM. Thus, there exists a need for more comprehensive works to understand the energy decay and cluster growth in the general dimension, for this model. There has been, indeed, recent [25,26] interest along this direction, to verify whether the energy exponent θ is $d/2$, that can be obtained from the Burger's equation, or it is $2d/(d+2)$, a consequence of ballistic aggregation. Furthermore, the picture with respect to the cluster growth in d dimensions, and its connection, if any, with the energy decay, is rather unclear and much less attended due to technical reasons. In this work, we undertake a detailed study with the aim of obtaining a clearer picture with respect to both the quantities.

The objectives of this paper, thus, are to investigate the correctness of the hyperscaling relation of Eq. (4), for the BAM in $d = 2$ and 3, and check if at least an analogous picture exists for the connection between the decay of energy and the growth of mass in the GGM. To verify the hyperscaling relation [4] in the BAM, as stated above, we consider different packing fractions. We observe that the relation is valid irrespective of the dimension and packing fraction. In the high density limit, in addition, the prediction of Eq. (1) appears correct. This is because of the fact, as already mentioned, that the collisions are more random and thus velocities are uncorrelated in a high density situation. On the other hand, the results for the GGM does not provide any hint of the existence of a relation of this type. In this case, even though dimension dependence of energy decay matches the CPY picture [1,2,5], the growth of mass appears rather insensitive to d.

Note here that in the above discussions t represents real time. In the literature of GGM, often time has been expressed in terms of number of collisions per particle (τ). In the clustering regime, linear relation between these has been reported [31,33]. In the pre-clustering regime [33], to be discussed later, τ has a logarithmic dependence on t.

The rest of the paper is organized as follows. In Sec. II we provide more details on the theoretical predictions for the BAM. Models and methods are discussed in Sec. III. Results are presented in Sec. IV. Finally, Sec. V concludes the paper with a brief summary and outlook.

II. THEORETICAL BACKGROUND ON BAM

While originally derived from a different approach [1], Eq. (1) can also be obtained by starting from the kinetic equation [4,7,24–27]

$$\frac{dn}{dt} = -\text{“collision cross section”} \times v_{\rm rms} \times n^2, \tag{5}$$

where n is the particle or cluster density and $v_{\rm rms}$ is the root-mean-squared velocity of the particles. The collision cross section is proportional to ℓ^{d-1}, where ℓ, for spherical particles, can be taken to be their average diameter, which scales with the average mass as $m^{1/d}$. The particle density, given that the total mass is conserved, scales inversely with the average mass, i.e.,

$$n \propto \frac{1}{m}. \tag{6}$$

Incorporation of these facts in Eq. (5) leads to

$$\frac{dm}{dt} \sim m^{(d-1)/d} v_{\rm rms}. \tag{7}$$

For uncorrelated velocity one can take [4,24,26]

$$v_{\rm rms} \sim m^{-1/2}, \tag{8}$$

to write

$$\frac{dm}{dt} \sim m^{(d-2)/2d}. \tag{9}$$

Solution of Eq. (9) provides time dependence of mass in Eq. (1). However, a deviation from Eq. (8) can invalidate the predictions in Eq. (1). For $v_{\rm rms} \sim m^{-z}$, the growth exponent ζ becomes [25]

$$\zeta = \frac{d}{1+dz}. \tag{10}$$

From Eq. (7), using the time dependence of energy from Eq. (2), and that of mass from Eq. (3), after considering that $v_{\rm rms} \sim E^{1/2}$, one arrives at

$$t^{\zeta-1} = t^{(2\zeta d - 2\zeta - \theta d)/2d}, \tag{11}$$

by discarding prefactor(s). Simple power counting provides the hyperscaling relation [4] of Eq. (4). Equation (4) in $d = 1$, 2, and 3 reads

$$\theta + 2\zeta = 2, \tag{12}$$

$$\theta + \zeta = 2, \tag{13}$$

and

$$3\theta + 2\zeta = 6, \tag{14}$$

respectively. We intend to verify these equations for the BAM. We have obtained the time dependence of mass in Eq. (1) by considering Eq. (8). When this is used in Eq. (4), it straightforwardly appears that mass and energy relate to each other inversely.

III. MODELS AND METHODS

For both the models, hard spherical particles, mass being uniformly distributed over the volume or area of the objects, move freely between collisions [4,13]. Mass and momentum remain conserved during the collisions. For the BAM, even though the size of the new particle increases, its shape is kept unchanged. For example, two initial spheres of masses and diameters (m_i,σ_i) and (m_j,σ_j), respectively, coalesce to form a single sphere of mass

$$m' = m_i + m_j, \tag{15}$$

with diameter [4]

$$\sigma' = \left(\sigma_i^d + \sigma_j^d\right)^{1/d}. \tag{16}$$

In this shape retaining process, if the new sphere overlaps with any other particle, then this event is treated as another collision and the same method of update is applied. The position ($\vec{r}'$) of the center of mass and the velocity ($\vec{v}'$) of the new particle can be obtained from the conservation equations [8]

$$m'\vec{r}' = m_i\vec{r}_i + m_j\vec{r}_j, \tag{17}$$

and

$$m'\vec{v}' = m_i\vec{v}_i + m_j\vec{v}_j, \tag{18}$$

where $\vec{r}_i$ and $\vec{r}_j$ are the positions and $\vec{v}_i$ and $\vec{v}_j$ are the velocities of particles i and j, respectively, before the collision.

In the case of the GGM, the particle velocities are updated via [8,13]

$$\vec{v}_i' = \vec{v}_i - \left(\frac{1+e}{2}\right)[\hat{n}\cdot(\vec{v}_i - \vec{v}_j)]\hat{n} \tag{19}$$

and

$$\vec{v}_j' = \vec{v}_j - \left(\frac{1+e}{2}\right)[\hat{n}\cdot(\vec{v}_j - \vec{v}_i)]\hat{n}, \tag{20}$$

where $\vec{v}_i'$ and $\vec{v}_j'$ are the postcollisional velocities. In Eqs. (19) and (20) $\hat{n}$ represents the unit vector parallel to the relative position of the particles i and j. In this case, since the colliding particles do not undergo coalescence, the particle mass remains unchanged throughout the evolution.

We perform event-driven molecular dynamics simulations with these models [35,36], where an event is a collision. In this method, since there is no interparticle interaction or external potential, particles move with constant velocities till the next collision. Time and partners for the collisions are appropriately identified [36]. Inelastic collapse [15], a well known problem for GGM, was avoided by assigning the value of e to unity, whenever needed, for relative velocity of the colliding partners less than a cutoff value for which we chose the number 10^{-4}.

All the results are obtained from simulations in periodic boxes of linear dimension L (equal in all directions), in units of the starting particle diameter (see below). Quantitative results are presented after averaging over multiple independent initial configurations, the numbers lying between 5 and 15. We start with random initial configurations for both positions and velocities, with $\sigma_i = 1$ for all particles. The packing fractions (ϕ), values of which will be mentioned later, are calculated as $\phi = (N/L^d) \times x$, where N is the initial number of particles in a box, and $x = 1, \pi/4$, and $\pi/6$ in $d = 1, 2$, and 3, respectively. While the values of N will be specified again in appropriate places, here we mention that this number is 10^5 for the BAM in all studied spatial dimensions, and 9830, 97 000, and 310 000 for the GGM in $d = 1, 2$, and 3, respectively, at least for all the quantitative results. These numbers are large and our results, within the presented time range, do not suffer from finite-size effects. In the case of BAM the number of particles decreases with time. So, for this model the specified numbers certainly correspond to the values at the beginning of the simulations.

In both the cases, the average mass of clusters is calculated as

$$m = \left[\sum_{j=1}^{N_c(t)} C(j,t)\right]^{-1}\left[\sum_{j=1}^{N_c(t)} jC(j,t)\right], \tag{21}$$

where $C(j,t)$ is the number of clusters of size j and $N_c(t)$ is the size of the largest cluster, at time t. Even though the results will primarily be presented from this definition (unless otherwise mentioned), we have calculated m from alternative definitions as well, which will be mentioned in the appropriate place.

While in the case of the BAM the information on the mass of a cluster is carried by the size of the particles, for the GGM appropriate identification of the clusters is needed. For the latter case, it was done [25] by appropriately marking the closed cluster boundaries within which the packing fraction is higher than a cutoff number ϕ_c ($\simeq$0.5 in $d = 1$, $\simeq$0.31 in $d = 2$, and $\simeq$0.21 in $d = 3$). Of course, the mass of a cluster will depend upon the choice of ϕ_c. We will later demonstrate that different choices, nevertheless, lead to the same growth exponent.

IV. RESULTS

We divide this section into three parts. The first two subsections contain the BAM results from $d = 2$ and $d = 3$. The GGM results are presented in the last one.

A. BAM in $d = 2$

In Fig. 1 we show two snapshots, obtained during an evolution in the two-dimensional (2D) BAM. These snapshots are from late enough times so that the clusters are reasonably well grown. All the droplets, particularly the smaller ones, may not appear perfectly circular. This is because of a technical reason—we have divided the whole space to form a discrete lattice system and marked the sites that fall within the boundary of one or the other droplet. It is clear from these figures that the number of clusters is decreasing with time and thus, the average mass of the clusters is increasing.

In Fig. 2(a) we plot the energy (normalized to unity at $t = 0$) for three different packing fractions, viz., $\phi = 0.004$, 0.08, and 0.4, versus time, on a log-log scale. Figure 2(b) shows the log-log plots of the growth of mass for the same three values of ϕ. While the trends in the long time limit are consistent

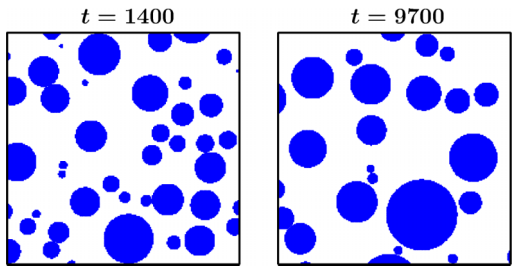

FIG. 1. Snapshots during an evolution in the two-dimensional BAM, for the packing fraction $\phi = 0.08$. The times are mentioned on the top of the frames. The simulation box size is $L = 1024$, containing 10^5 particles. For both the times only parts of the original system have been shown.

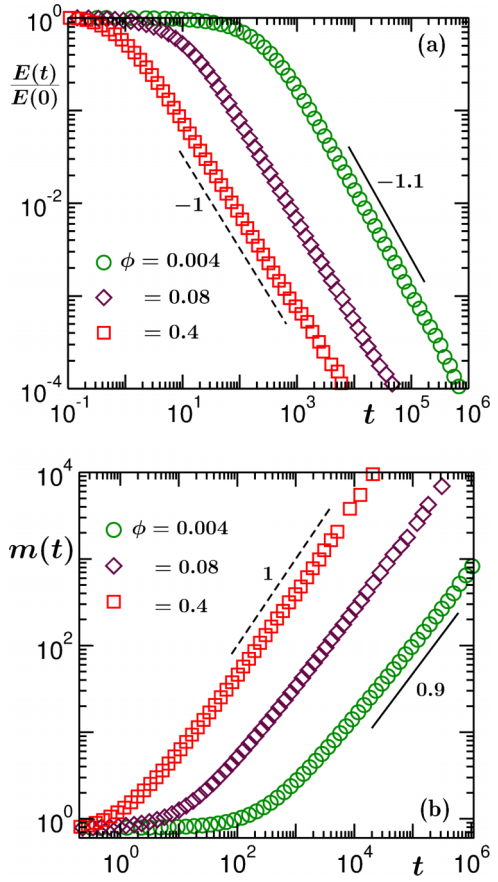

FIG. 2. Log-log plots of (a) energy vs time and (b) mass vs time, for different packing fractions (mentioned in the figure). The solid and dashed lines represent power laws. Corresponding exponents are mentioned. All results correspond to the BAM in $d = 2$. These and other quantitative results for the BAM are obtained for $N = 10^5$.

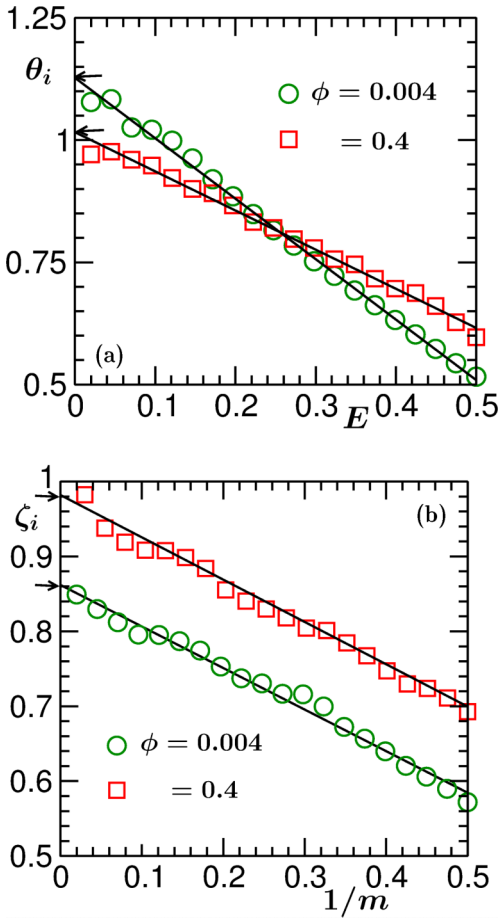

FIG. 3. Plots of (a) θ_i vs E and (b) ζ_i vs $1/m$, for two values of the packing fraction. The results correspond to the BAM in $d = 2$. Continuous lines are linear fits to the simulation data sets. The arrows point towards the asymptotic values.

with power laws, θ and ζ, the corresponding exponents for the energy decay and growth of mass, respectively, for some densities differ from each other, as well as from the CPY [1] value 1 (recall that we are working in $d = 2$). The deviations from the CPY value are quite significant when ϕ is small. The value of ζ increases towards unity [4] with the increase of ϕ. On the other hand, θ decreases from a higher value, towards unity, for a similar change in ϕ. This already provides a hint on the validity of the hyperscaling relation [4]. Here note that a conclusion on the power-law exponent from log-log plots or simple data fitting exercises can be misleading, particularly when data over many decades (without being affected by the finite size of the systems) are unavailable. This is because of the presence of an offset before the data reach the expected scaling regime. Thus, to accurately quantify the exponents and confirm the validity of Eq. (4) [Eq. (13) in $d = 2$] we need more accurate quantitative analysis.

For this purpose, we calculate the instantaneous exponent θ_i, for the decay of E, defined as [37]

$$\theta_i = -\frac{d(\ln E)}{d(\ln t)}, \tag{22}$$

accepting that a power-law behavior indeed exists. In Fig. 3(a) we plot θ_i as a function of E. For the sake of clarity, here we show the plots for $\phi = 0.004$ and 0.4 only. In both cases linear behavior is visible, over an extended range. We extract the asymptotic value θ from the convergence of θ_i in $t \to \infty$, i.e., the $E \to 0$ limit. Indeed, θ exhibits density dependence.

A similar exercise has also been performed for the growth of mass. In Fig. 3(b) we plot the instantaneous exponent ζ_i, for the growth of mass, defined as [37]

$$\zeta_i = \frac{d(\ln m)}{d(\ln t)}, \tag{23}$$

as a function of $1/m$, for $\phi = 0.004$ and 0.4. Here also we obtain asymptotic values from linear extrapolations. Clearly, the numbers vary with the change in ϕ. The exponents θ and ζ, obtained from these exercises, for different values of ϕ, are quoted in Table I.

CPY [1] predict that the energy decay and the growth of mass are inversely proportional to each other, with $\theta = \zeta = 1$. Our results show that the exponents, which have been accurately quantified via the calculation of instantaneous exponents [37], are nonuniversal, with strong dependence upon the packing fraction. We observe that the CPY predictions tend to be valid only at higher values of ϕ. For lower values of ϕ there exist significant deviations. But the simulation results follow the relation [4] $\theta + \zeta = 2$, to a good accuracy—see

TABLE I. Values of θ and ζ are listed for different packing fractions, for the 2D BAM.

ϕ	θ	ζ	$\theta+\zeta$
0.004	1.13	0.86	1.99
0.08	1.08	0.91	1.99
0.24	1.07	0.94	2.01
0.31	1.03	0.97	2.00
0.4	1.01	0.98	1.99
0.44	1.01	0.99	2.00

the numbers quoted in the last column of Table I. While the numbers in Table I provide accurate information, to get a feel about how the convergence towards the CPY exponent occurs, in Fig. 4(a) we show plots of θ and ζ, versus ϕ.

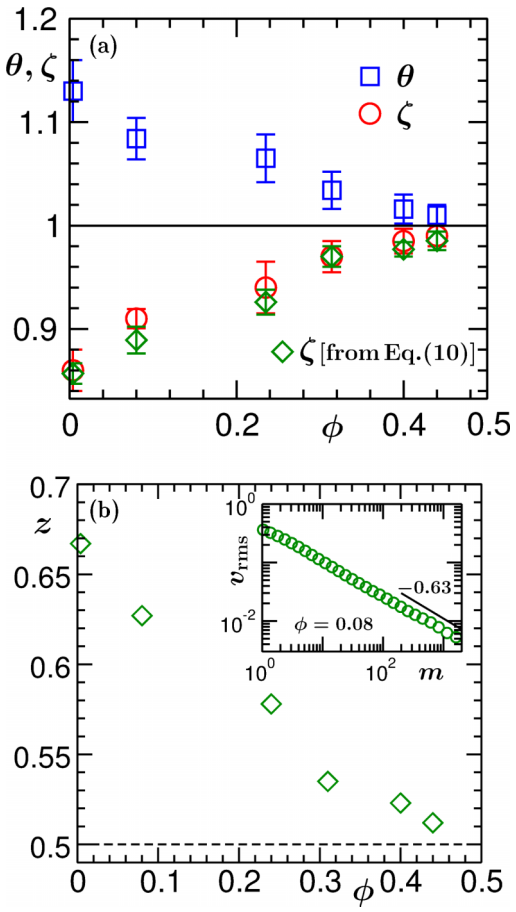

FIG. 4. (a) Exponents θ and ζ are plotted vs ϕ. The horizontal line marks the CPY value. For ζ, we have also included results obtained from Eq. (10). (b) Values of the exponent z (related to the dependence of $v_{\rm rms}$ on m) have been plotted vs ϕ. The dashed horizontal line marks the value 0.5. Inset: Log-log plot of $v_{\rm rms}$ vs m, for $\phi = 0.08$. The solid line there corresponds to a power law, the exponent for which has been mentioned. All results are for the 2D BAM. The error bars here and in other places are estimated as the standard deviation in a set of asymptotic values of exponent, for a particular value of ϕ, obtained via piecewise linear fits of the instantaneous exponents (by dividing the data sets into multiple parts) such as the ones presented in Fig. 3.

In Fig. 4(a) we have also presented data for ζ which were estimated via Eq. (10). This data set shows a similar trend as the one obtained via the calculation of ζ_i. To apply Eq. (10), we have estimated z by calculating $v_{\rm rms}$ at different times. A plot of z as a function of ϕ is shown in Fig. 4(b). In the inset of Fig. 4(b) we presented a log-log plot of $v_{\rm rms}$ vs m, for $\phi = 0.08$. The solid line there, consistent with the simulation data, represents a power law with exponent $z = 0.63$, that differs significantly from 0.5 that is needed to validate the prediction of CPY. Here note that z was estimated via fitting of the data in the inset to a power-law form. From the main frame of Fig. 4(b) we notice that z deviates from 0.5 even when $\phi = 0.45$.

While these results of ours are consistent with previous reports [4], such accurate analyses are new. On the other hand, in $d = 3$ a simulation study to confirm the validity of the hyperscaling relation was not performed earlier, to the best of our knowledge. In the next subsection we present these results.

Before moving to the next subsection, we provide further discussions on the $d = 2$ results which may be valid in $d = 3$ as well. We have accepted the linear behavior of the data sets in Fig. 3, for energy as well as mass. Given the statistical fluctuation in the presented results, further checks of this assumption are necessary. Moreover, what scaling forms do such linear trends imply?

For a linear behavior of the θ_i versus E data, one can use

$$\theta_i = \theta - AE, \tag{24}$$

in the definition in Eq. (22), to write

$$\frac{dE}{AE^2 - \theta E} = \frac{dt}{t}, \tag{25}$$

where A is the slope of a θ_i versus E plot and $AE < \theta$. Then Eq. (25) provides

$$E = \frac{\theta/A}{1 + a_0 t^{\theta}}, \tag{26}$$

where a_0 is a positive constant. This implies that the value of E at $t = 0$ provides a nonzero slope in Fig. 3(a) and this ofset is also responsible for the misleading trend of E versus t data on a double-log scale, over early decades. However, this scaling form will be completely true if a linear behavior in Fig. 3(a) is realized from $t = 0$. This, in fact, is not the case. For $E > 0.5$ there exists slight bending (data not shown). This implies a correction to the form in Eq. (26). Furthermore, had there been no correction, the data sets in Fig. 3(a) would have been described by

$$\theta_i = \theta(1 - E), \tag{27}$$

implying same values for the y intercept and the slope, i.e.,

$$A = \theta. \tag{28}$$

This fact, in absence of a correction, automatically leads to the initial condition $E = 1$ at $t = 0$. Here recall that everywhere we have normalized E by its value at $t = 0$. Equation (27) can also be checked by using Eqs. (26) and (28) in Eq. (22). However, in reality small disagreement exists between A and θ, when we fit the data sets in Fig. 3(a) to the form in Eq. (24).

In Fig. 5(a) we have shown a comparison between the simulation data and fit to the mathematical form in Eq. (26), for $\phi = 0.24$, by fixing the corresponding value of θ to the

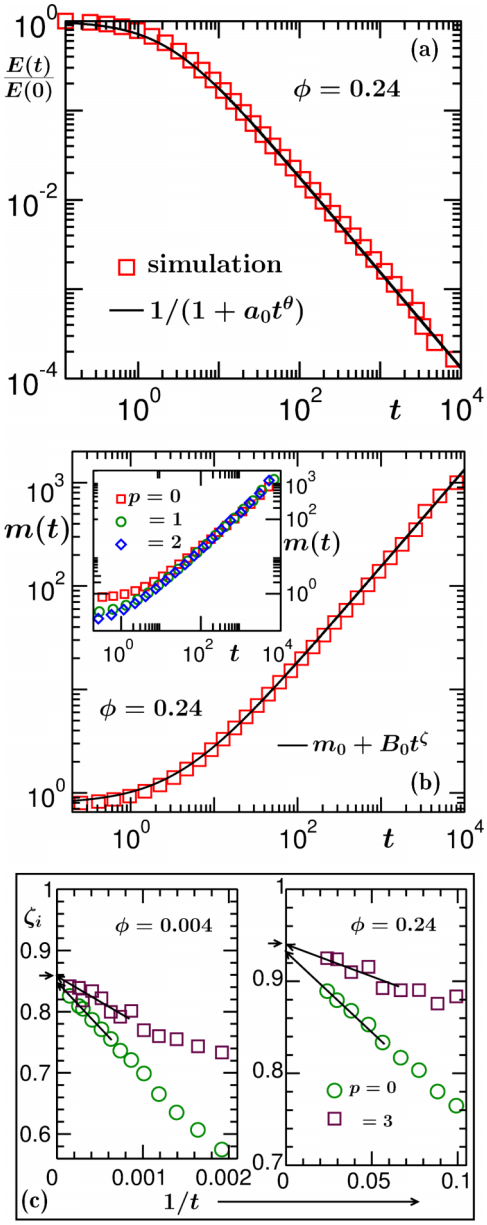

FIG. 5. (a) Energy is plotted vs time, on a log-log scale, for the 2D BAM with $\phi = 0.24$. The solid curve corresponds to a fitting to Eq. (26). (b) Same as (a) but for m. The solid line here represents Eq. (29). In the inset of (b) we show comparison of m, obtained by using Eq. (30), for $p = 0$, 1, and 2. The ordinates of the data sets corresponding to $p = 1$ and 2 have been appropriately scaled to superimpose them with the $p = 0$ one in the late time regime. (c) Plots of ζ_i vs $1/t$ for two different values of p, mentioned in the figure, for $\phi = 0.004$ and 0.24. While the arrows outside the frames are located at the values of ζ quoted in Table I, the arrowheaded lines (inside the frames) are guides to the eye.

number mentioned in Table I and asserting that $\theta = A$. A near perfect agreement is observed. This substantiates the linear assumption in Fig. 3(a), as well as confirms the absence of any strong correction in the early time decay. This is consistent with the fact that θ/A differs from unity by approximately 10%. Nevertheless, we state here that while the empirical derivation provides Eq. (26), any correction of the type $(a + t)^{-\theta}$ cannot be ruled out. Even though the asymptotic values of the exponent systematically deviate from unity, for the range of density considered in this work, the largest deviation is approximately 0.15. In such a situation the above correction cannot be accurately separated from the form in Eq. (26).

Similarly, considering the linear trend in Fig. 3(b), one obtains

$$m = m_0 + B_0 t^\zeta, \tag{29}$$

where B_0 is a constant amplitude and m_0 is the average initial mass. In Fig. 5(b) we show an exercise, analogous to Fig. 5(a), by fitting simulation data for mass to Eq. (29). Here the continuous line is obtained by fixing m_0 to $\pi/4$ (which indeed is the starting mass), ζ to the value quoted in Table I corresponding to $\phi = 0.24$, and using B_0 as an adjustable parameter. Once again, the agreement is nice, validating the linear assumption and discarding any possibility of a strong correction. Here we mention that in the literature of growth kinetics, such linear trends in the time-dependent exponents have been misinterpreted as strong corrections to scaling—see Refs. [38,39] for discussion.

As mentioned earlier, while we have calculated m from the definition in Eq. (21), we have also obtained it from [40]

$$m = \left[\sum_{j=1}^{N_c(t)} j^p C(j,t)\right]^{-1} \left[\sum_{j=1}^{N_c(t)} j^{p+1} C(j,t)\right], \tag{30}$$

with $p = 1$, 2, and 3. Note that the definition in Eq. (21) corresponds to $p = 0$. A comparative picture is presented in the inset of Fig. 5(b) with $p = 0$, 1, and 2, for $\phi = 0.24$. As expected, the results for larger p are less prone to initial bending. This fact can be further appreciated from Fig. 5(c) where, for $\phi = 0.004$ and 0.24, we have plotted ζ_i versus $1/t$ for $p = 0$ and 3. Certainly, the data sets for $p = 3$ exhibit weaker variation as a function of time. Given that data for both the values of p essentially converge to the same asymptotic numbers, this exercise provides additional confidence with respect to the corresponding numbers quoted in Table I. This consistency has been checked for various other values of ϕ in both the dimensions to establish the validity of the hyperscaling relation. Since the results in the asymptotic limit remain unchanged, we will stick to the former definition from here on. Another reason for choosing $p = 0$ is that for higher p the data for the instantaneous exponent exhibit stronger statistical fluctuation.

B. BAM in $d = 3$

Given that the context is the same and primary discussions have been provided in the previous subsection, here we straightaway present the results. First, in Fig. 6 we show a snapshot for the 3D BAM evolution. Like in $d = 2$, here also the lesser sphericity is visible for smaller particles. This is because of the technical reason mentioned in the previous subsection.

In Fig. 7(a) we plot the energy as a function of time, on a log-log scale, for various different choices of the packing fraction. Prediction of CPY [1] for the exponent for the energy decay, as well as that for the growth of mass, is 6/5 in this space dimension. The values of θ, as can be judged from Fig. 7(a), do

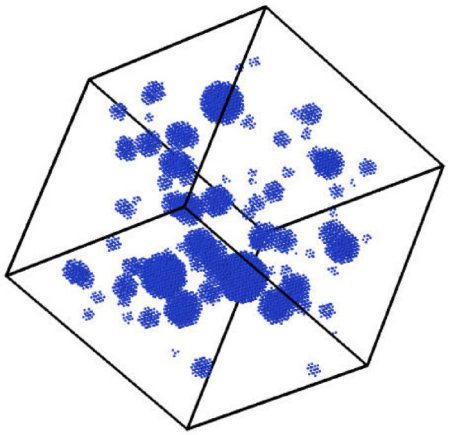

FIG. 6. An evolution snapshot for the 3D BAM, from $t = 100$. The packing fraction and the linear dimension of the cubic box are 0.052 and 64, respectively.

not obey this theoretical number for all values of ϕ, like in $d = 2$. In this dimension also θ seems to be decreasing from a higher value towards 6/5 as the packing fraction increases. In Fig. 7(b) we show log-log plots of average mass of the clusters as a function of time, for the same choices of the packing fraction. Unlike the energy decay, here the value of the exponent ζ

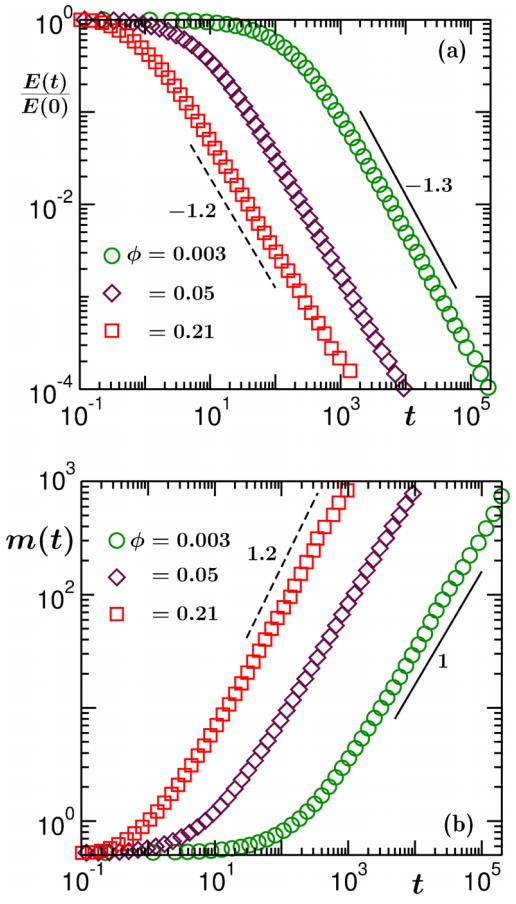

FIG. 7. Log-log plots of (a) energy vs time and (b) mass vs time, for the 3D BAM. Results from three different packing fractions are included. The solid and dashed lines are power laws, exponents for which are mentioned.

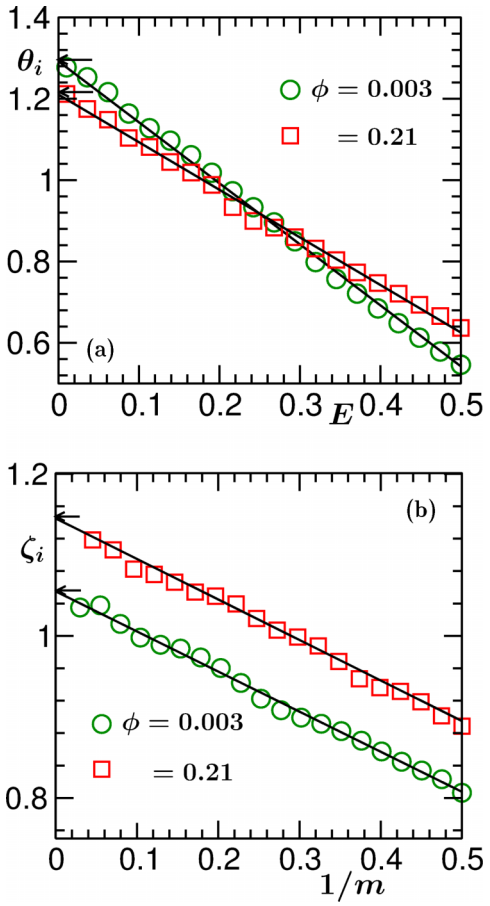

FIG. 8. Plots of the instantaneous exponents (a) θ_i and (b) ζ_i, vs E and $1/m$, respectively, for the 3D BAM. The solid straight lines are linear fits to the simulation data sets. The arrows mark the asymptotic values. We have shown results from two values of ϕ.

increases towards the value 6/5 with the increase of ϕ. This fact is also similar to the case of $d = 2$.

For more accurate quantification of the exponents, for the energy decay as well as for the growth of mass, we calculate the instantaneous exponents [37] θ_i and ζ_i, defined earlier, and plot them versus E and $1/m$, respectively, in Figs. 8(a) and 8(b), for $\phi = 0.003$ and 0.21. The asymptotic values, estimated from these plots of instantaneous exponents, by assuming linear behavior of the data sets, are quoted in Table II. It can be observed that, like in $d = 2$, the exponents are strongly ϕ dependent. However, they obey the relation [4] $3\theta + 2\zeta = 6$, within about 1% deviation. Again, for a visual feeling, in Fig. 9(a) we show θ and ζ with the variation of ϕ.

TABLE II. Values of θ and ζ for different packing fractions. All results are for 3D BAM.

ϕ	θ	ζ	$3\theta + 2\zeta$
0.003	1.29	1.05	5.97
0.05	1.25	1.10	5.95
0.16	1.22	1.14	5.94
0.21	1.21	1.15	5.93
0.26	1.2	1.17	5.94

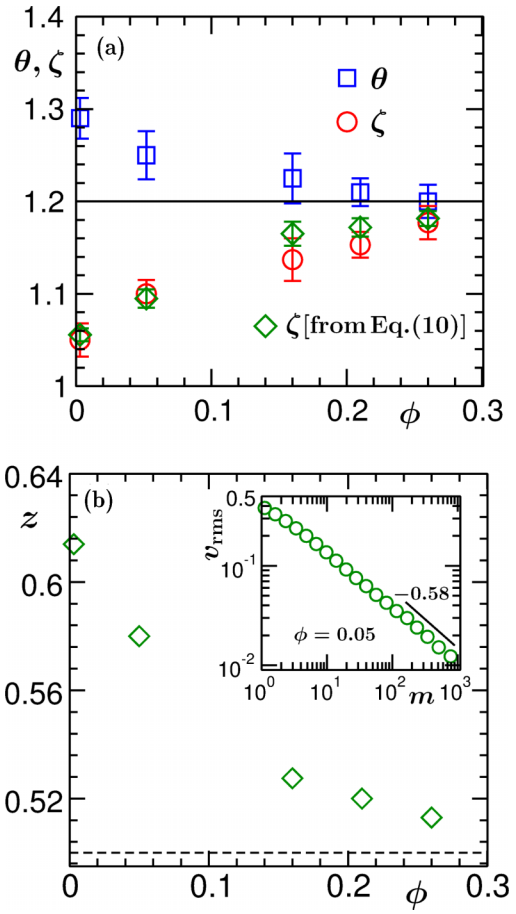

FIG. 9. (a) Exponents θ and ζ are plotted vs ϕ. The horizontal line represents the CPY value. Values of ζ calculated from Eq. (10) are also included. (b) Exponent z is plotted vs ϕ. Dashed horizontal line there corresponds the value 0.5. Inset shows a log-log plot of $v_{\rm rms}$ vs m, for $\phi = 0.05$. The solid line there corresponds to a power law, the exponent for which is mentioned. All results correspond to the 3D BAM.

In this dimension also, for ζ, we have shown results from calculations via Eq. (10). Again, trends of the data sets, obtained via convergence of ζ_i and from Eq. (10), are very similar. A plot of z vs ϕ is shown in Fig. 9(b). The inset of this figure demonstrates the consistency of the $v_{\rm rms}$ vs m data with the estimated exponent, for $\phi = 0.05$.

Thus, the hyperscaling relation [Eq. (14)] is valid, to a good accuracy, for all values of ϕ and the CPY exponent appears reasonably accurate only for high packing fraction. The critical numbers turn out to be $\phi \gtrsim 0.45$ and $\gtrsim 0.25$, respectively, in $d = 2$ and 3, by considering that 2% deviation from the CPY value as acceptable. Here note that in $d = 1$, CPY and, thus, the hyperscaling relation are observed to be valid for all previously studied densities [1,25].

Like in the 2D case, θ_i vs E curves show a nice linear trend in $d = 3$ also, for $E \leqslant 0.5$. This implies the validity of Eq. (26) over the most part of the energy decay. A similar conclusion applies to the case of mass. We have indeed checked the accuracy of Eqs. (26) and (29) by comparing them with the simulation data for E versus t and m versus t. Excellent agreements have been observed. However, for the sake of brevity we do not present these results.

C. The case of GGM

As stated earlier, even though the particles do not stick to each other, inelastic collisions lead to clustering in the GGM. However, unlike in the case of the BAM, in this case, over an initial period of time, referred to as the homogeneous cooling state (HCS) [13], the density in the system remains uniform. After a certain time, the value of which depends upon the overall density of particles and the choice of e, the system falls unstable to fluctuations and crosses over to a clustering regime, referred to as the inhomogeneous cooling state (ICS) [13]. In the HCS the energy decay follows Haff's law [41],

$$E = (1 + ct)^{-2}, \tag{31}$$

where c is a dimension dependent constant. While the decay in the HCS, apart from c, is dimension independent, it has been established that the exponent in the ICS is strongly dimension dependent [15,25,27,28,32–34]. On the other hand, no appropriate conclusion has been drawn [25,29–31,42,43] with respect to the dimension dependence of the growth of the average mass of clusters. In this subsection, while the primary objective is to investigate the latter issue in the GGM, we present results for the decay of energy also. For both quantities our focus will be on the ICS.

We start by showing a representative snapshot, in Fig. 10, from the evolution in the GGM in $d = 3$, for $e = 0.8$ and $\phi = 0.1$. The snapshot shows high and low density regions, like the phase separation during a vapor-liquid (VL) transition [11]. The morphology here is interconnected, and resembles the ones for high overall density (close to the critical value) in the VL transitions [11]. Nevertheless, there exist differences. The equal-time correlation function [44], that provides quantitative information on pattern formation, does not [29,30] exhibit intermediate distance oscillation (around zero) in the GGM as strong as that for the VL transition [11,45]. A reason behind such a structural difference is that, while in the VL transition phase separation is driven by interparticle interaction, the clustering in the GGM is related to the velocity parallelization due to inelastic collisions. That way, the structure, and thus, the correlation function for the GGM, should have more similarity with that for the active matter systems where the direction

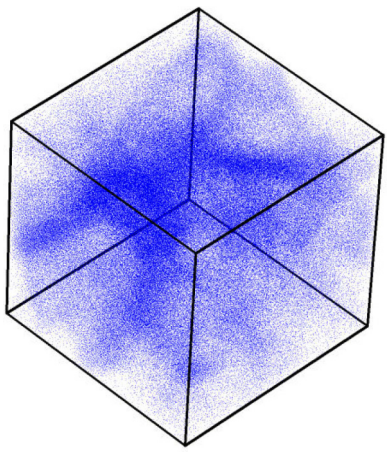

FIG. 10. An evolution snapshot for the 3D GGM with $e = 0.8$. The packing fraction is 0.1 and the linear dimension of the simulation box is $L = 120$. Locations of the particles are marked.

of motion of a particle is strongly influenced by the average direction of motion of the neighbors, e.g., in the Vicsek model [46,47]. In any case, given the structural difference between the GGM and the BAM, a similarity in the dynamics is not really expected. Below we substantiate this.

In Fig. 11(a) we show plots for the decay of energy, from $d = 1$, 2, and 3, for the GGM. See the caption for choices of parameters. Note that the axes are scaled to bring all the plots within appropriate abscissa and ordinate ranges that can help make the crucial features identifiable for all values of d. Clearly, the decay rate at late time (in the ICS) is different for different dimensions. Interestingly, the exponents are in nice agreement with $2d/(d+2)$, predicted by CPY [1]—see the consistency of the data sets with various power-law lines. At much later time (not shown) the decays are faster, which can be related to finite-size effects. The presented results are consistent with other simulation studies [15,25,28,32]. On the other hand, from some previous studies on growth of mass [25,31], we got a hint that this agreement of energy decay with the prediction of CPY [1] may be accidental and should have a different reason. To make a more concrete statement on this aspect, below we look at the growth picture. Before moving to that, in Fig. 11(b) we show a plot for θ_i from all three dimensions. The convergence in all the cases is quite consistent with the CPY numbers.

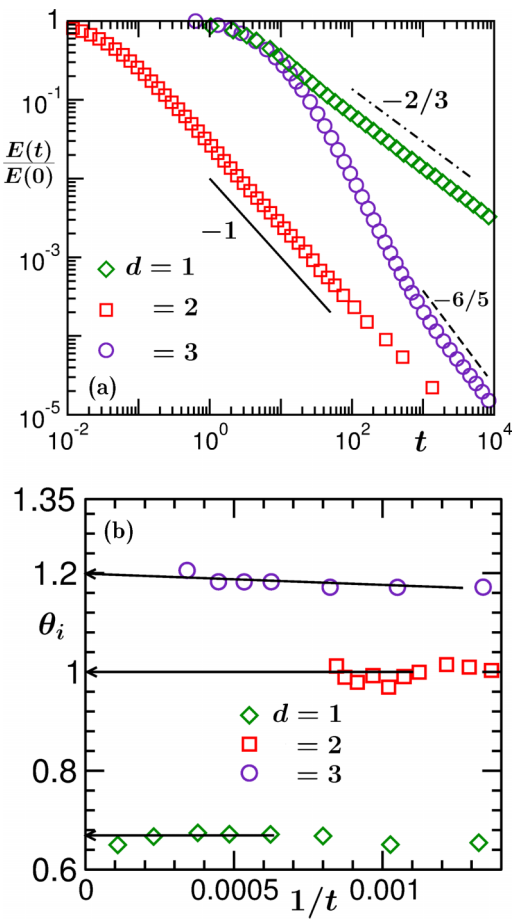

FIG. 11. (a) Log-log plots of the decay of energy in the GGM in $d = 1, 2,$ and 3. The dashed-dotted, dashed, and solid lines correspond to power laws, exponents for which are mentioned next to them. The presented results correspond to $\phi = 0.3$, 0.3, 0.1; $e = 0.5$, 0.9, 0.8; and $L = 32\,768$, 512, 120 for $d = 1$, 2, and 3, respectively. The corresponding numbers of particles are 9830, 97 000, and 310 000. The data sets have been multiplied by appropriate factors to bring them within the presented abscissa and ordinate scales. (b) Plots of θ_i vs $1/t$ in $d = 1$, 2, and 3. Here we have chosen a different value of e (0.2) for $d = 3$ than in (a) to access longer range of decay with $\theta = 6/5$. The arrowheaded lines point towards the CPY values.

In Fig. 12(a) we present plots of m versus t, on a log-log scale, for all three dimensions. We discard data affected by the finite size of the systems. Furthermore, like in the plots

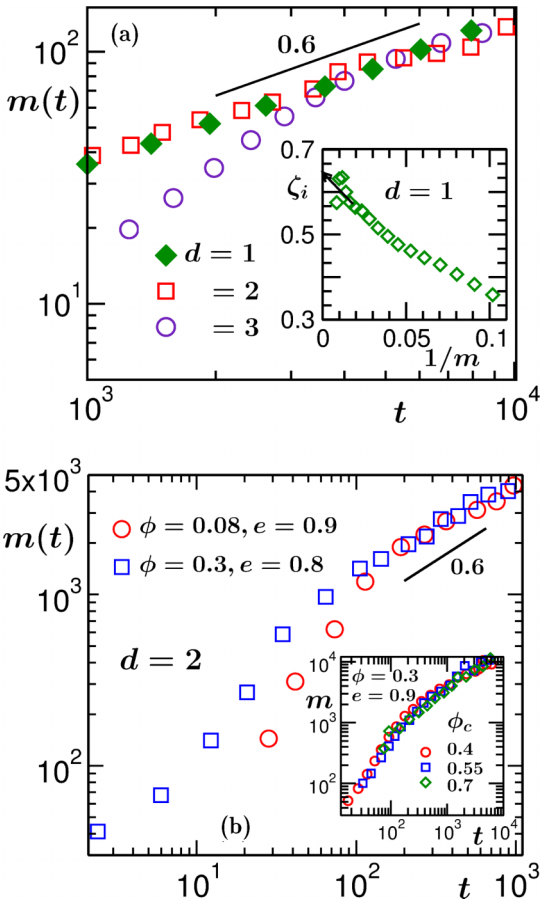

FIG. 12. (a) Log-log plots of the growth of the average mass in all the three dimensions for the GGM. The data sets have been multiplied by appropriate numbers to bring them onto the scales of the graph. The solid line corresponds to a power law with an exponent 0.6. The system sizes, coefficients of restitution, and packing fractions for different dimensions are same as in Fig. 11(a). The discrepancy of $d = 3$ data at early time is related to longer crossover time to ICS, for the chosen coefficient of restitution and density of particles. Inset: Plot of instantaneous exponent, ζ_i, vs $1/m$, for the 1D GGM. The solid line there is a guide to the eye. (b) Log-log plots of the growth of average mass for different combinations of coefficient of restitution and packing fraction, mentioned in the figure, in $d = 2$. The data set corresponding to $\phi = 0.08$ has been appropriately scaled to bring it within the presented ranges of the axes. The solid line there is a power law with an exponent 0.6. The inset in (b) shows plots of m vs t, in $d = 2$, for different choices of ϕ_c, quoted in the figure, for the case $\phi = 0.3$ and $e = 0.9$ (the ordinates have been appropriately scaled to superimpose the data sets).

of energy decay, data from different dimensions have been multiplied by different factors. It appears that all the data sets exhibit power laws, at late times, with a very similar exponent, which is close to $2/3$. In this log-log plot, however, the exponent appears a bit smaller than $2/3$, approximately 0.6. This may again be due to the offset before reaching the scaling regime. In the inset of this figure we have shown ζ_i as a function of $1/m$, for $d = 1$. The convergence appears closer to $2/3$. For the sake of clarity, we avoided showing similar results from $d = 2$ and 3, which show a similar trend in the direct plot (at late time). We mention here that because of strong finite-size effects [31] and difficulty in dealing with very large systems, the scaling regime is relatively small for $d = 3$.

This weak dependence of growth of mass on dimension not only invalidates equivalence between the GGM and the BAM in $d > 1$, it also suggests the absence of any hyperscaling relation of the type obeyed by the BAM results. We mention here that the GGM results do not depend upon the choices of different e or overall density, unlike in the BAM case. This fact we have demonstrated in Fig. 12(b) for the $d = 2$ case. There the results for different e and ϕ values exhibit similar power-law growth. These results are consistent with the finite-size scaling estimate of exponent ($\simeq$0.3) for the growth of average domain length [31].

As mentioned earlier, for the GGM, values of m will depend upon the choice of ϕ_c, the cutoff packing fraction to identify clusters. This indeed is the case. In the inset of Fig. 12(b) we show representative plots for different choices of ϕ_c. These results are from $d = 2$, with $\phi = 0.3$ and $e = 0.9$. To superimpose the data sets different multiplicative factors were needed for the ordinate. However, they all lead to the same growth exponent.

The need for a ϕ_c in the GGM is due to the fact that the clusters here are essentially regions with a high density of particles. True clusters can be realized by adding attractive potential in the model, if the kinetic energy is less than a threshold value. In this model energy can decay exponentially fast. Such works, in fact, have recently been reported [17,48]. In this case the role of fractality in the growth process can also be probed, as was recently done in kinetics of vapor-solid transition (via time-step driven molecular dynamics simulations) [7].

V. CONCLUSION

Via event-driven molecular dynamics simulations we have studied nonequilibrium dynamics in ballistic aggregation (BAM) [1,4] and granular gas (GGM) [13] models. We have presented accurate results on the energy decay and the growth of mass. These results are compared with the available theoretical predictions [1,4,33].

We observe that for both the models the above mentioned quantities exhibit power-law behavior as a function of time. For the BAM, the corresponding exponents exhibit density dependence. Nevertheless, these exponents satisfy a hyperscaling relation [4]. With the increase of density, the energy and mass get inversely related to each other, the exponent being strongly dimension dependent. This latter observation is consistent with the prediction of CPY [1]. As a physical reason behind the difference between the exponents for energy decay and cluster growth in the low packing fraction scenario, Trizac and Krapivsky [24] showed that, in this limit, the particles with kinetic energy larger than the mean undergo very frequent collisions, which enhances the dissipation.

For the GGM, from accurate analysis we show that the energy decay satisfies the prediction of CPY in all dimensions [1]. However, this is not always inversely related with the growth of mass. In fact the latter exhibits very weak dimension dependence. For this model we have presented results for different densities and coefficients of restitution as well. The results appear to be independent of these parameters. All these facts are in denial of an equivalence between the GGM and BAM, except for $d = 1$. Furthermore, the growth exponent in GGM does not match any known value for coarsening related to conserved order parameter dynamics [44], with [49] or without [50] hydrodynamics [51].

In the context of BAM, further interesting studies are related to aggregation and fragmentation [16,18,23]. Incorporation of fragmentation indeed can provide information on a more realistic scenario. In the future we intend to undertake comprehensive studies by including this fact.

ACKNOWLEDGMENTS

The authors thank the Department of Science and Technology, Government of India, for financial support. S.K.D. also acknowledges the Marie Curie Actions Plan of European Commission (FP7-PEOPLE-2013-IRSES Grant No. 612707, DIONICOS) as well as the International Centre for Theoretical Physics, Trieste, for partial support. S.P. is thankful to the UGC, Government of India, for a research fellowship.

[1] G. F. Carnevale, Y. Pomeau, and W. R. Young, Phys. Rev. Lett. **64**, 2913 (1990).
[2] E. Ben-Naim, S. Redner, and F. Leyvraz, Phys. Rev. Lett. **70**, 1890 (1993).
[3] E. Ben-Naim, P. L. Krapivsky, and S. Redner, Phys. Rev. E **50**, 822 (1994).
[4] E. Trizac and J.-P. Hansen, J. Stat. Phys. **82**, 1345 (1996).
[5] L. Frachebourg, Phys. Rev. Lett. **82**, 1502 (1999).
[6] J. Piasecki, E. Trizac, and M. Droz, Phys. Rev. E **66**, 066111 (2002).
[7] J. Midya and S. K. Das, Phys. Rev. Lett. **118**, 165701 (2017).
[8] N. V. Brilliantov and T. Poeschel, *Kinetic Theory of Granular Gases* (Oxford University Press, Oxford, 2004).
[9] K. Binder and D. Stauffer, Phys. Rev. Lett. **33**, 1006 (1974).
[10] K. Binder, Phys. Rev. B **15**, 4425 (1977).
[11] S. Roy and S. K. Das, Soft Matter **9**, 4178 (2013).
[12] R. Shimizu and H. Tanaka, Nat. Commun. **6**, 7407 (2015).
[13] I. Goldhirsch and G. Zanetti, Phys. Rev. Lett. **70**, 1619 (1993).
[14] R. R. Rogers and M. K. Yao, *A Short Course in Cloud Physics*, 3rd ed. (Butterworth Heinemann, Oxford, 1989).

[15] X. Nie, E. Ben-Naim, and S. Chen, Phys. Rev. Lett. **89**, 204301 (2002).
[16] L. Mattson, Planet. Space Sci. **133**, 107 (2016).
[17] S. Takada, K. Saitoh, and H. Hayakawa, Phys. Rev. E **94**, 012906 (2016).
[18] R. K. Rai and R. Botet, Mon. Not. R. Astron. Soc. **467**, 2009 (2017).
[19] R. Rongali and M. Alam, Phys. Rev. E **89**, 062201 (2014).
[20] N. V. Brilliantov and F. Spahn, Math. Comput. Simul. **72**, 93 (2006).
[21] N. V. Brilliantov, A. S. Bodrova, and P. L. Krapivsky, J. Stat. Mech. (2009) P06011.
[22] F. Spahn, N. Albers, M. Sremcevic, and C. Thornton, Europhys. Lett. **67**, 545 (2004).
[23] N. V. Brilliantov, P. L. Krapivsky, A. Bodrova, F. Spahn, H. Hayakawa, V. Stadnichuk, and J. Schmidt, Proc. Natl. Acad. Sci. USA **112**, 9536 (2015).
[24] E. Trizac and P. L. Krapivsky, Phys. Rev. Lett. **91**, 218302 (2003).
[25] S. Paul and S. K. Das, Phys. Rev. E **96**, 012105 (2017).
[26] S. N. Pathak, D. Das, and R. Rajesh, Europhys. Lett. **107**, 44001 (2014).
[27] S. N. Pathak, Z. Jabeen, D. Das, and R. Rajesh, Phys. Rev. Lett. **112**, 038001 (2014).
[28] E. Ben-Naim, S. Y. Chen, G. D. Doolen, and S. Redner, Phys. Rev. Lett. **83**, 4069 (1999).
[29] S. K. Das and S. Puri, Europhys. Lett. **61**, 749 (2003).
[30] S. K. Das and S. Puri, Phys. Rev. E **68**, 011302 (2003).
[31] S. Paul and S. K. Das, Europhys. Lett. **108**, 66001 (2014).
[32] M. Shinde, D. Das, and R. Rajesh, Phys. Rev. E **79**, 021303 (2009).
[33] R. Brito and M. H. Ernst, Europhys. Lett. **43**, 497 (1998).
[34] S. Chen, Y. Deng, X. Nie, and Y. Tu, Phys. Lett. A **269**, 218 (2000).
[35] D. C. Rapaport, *The Art of Molecular Dynamics Simulations* (Cambridge University Press, Cambridge, England, 2004).
[36] M. P. Allen and D. J. Tildesley, *Computer Simulations of Liquids* (Clarendon Press, Oxford, 1987).
[37] D. A. Huse, Phys. Rev. B **34**, 7845 (1986).
[38] J. G. Amar, F. E. Sullivan, and R. D. Mountain, Phys. Rev. B **37**, 196 (1988).
[39] S. Majumder and S. K. Das, Phys. Rev. E **81**, 050102 (2010).
[40] G. R. Price, Ann. Hum. Genet. **35**, 485 (1972).
[41] P. K. Haff, J. Fluid Mech. **134**, 401 (1983).
[42] S. Luding and H. J. Herrmann, Chaos **9**, 673 (1999).
[43] S. Miller and S. Luding, Phys. Rev. E **69**, 031305 (2004).
[44] A. J. Bray, Adv. Phys. **51**, 481 (2002).
[45] S. K. Das and S. Puri, Phys. Rev. E **65**, 026141 (2002).
[46] T. Vicsek, A. Czirôk, E. Ben-Jacob, I. Cohen, and O. Shochet, Phys. Rev. Lett. **75**, 1226 (1995).
[47] S. K. Das, J. Chem. Phys. **146**, 044902 (2017).
[48] E. Murphy and S. Subramaniam, Phys. Fluids **27**, 043301 (2015).
[49] E. D. Siggia, Phys. Rev. A **20**, 595 (1979).
[50] I. M. Lifshitz and V. V. Slyozov, J. Phys. Chem. Solids **19**, 35 (1961).
[51] J.-P. Hansen and I. R. McDonald, *Theory of Simple Liquids* (Academic Press, London, 2008).